Phenomenological transition amplitudes in selected $1p$-shell nuclei

B. C. Doyle* and Nimai C. Mukhopadhyay
Department of Physics, Rensselaer Polytechnic Institute, Troy, New York 12180
(Received 26 August 1994)

We critically examine, in selected $1p$-shell nuclei, the theoretical procedure of determining nuclear transition matrix elements, by fits to low-energy electromagnetic and weak observables. We systematically study various fitting strategies using the latest database, and obtain a set of optimal one-body matrix elements. The onset of inadequacies of these sets in describing a given nuclear electroweak observable usually signals the breakdown of the $1p$-shell model and/or importance of the two-body corrections. We compare the particle-hole conjugate nuclei ^{6}Li and ^{14}N, and obtain effective amplitudes. We also study the mass-12 case and find a set of effective one-body amplitudes. The difference in the $p_{1/2}$ and $p_{3/2}$ radial wave functions plays an important role in our fits.

PACS number(s): 23.20.Js, 23.40.−s, 27.20.+n

I. INTRODUCTION

A very useful theoretical approach in nuclear structure physics, originally stressed by Donnelly and Walecka [1], has been to determine effective one-body amplitudes from a fit to the experimental electroweak data at small momentum transfer. This procedure has met with considerable success [1] in some "$1p$ shell" nuclei, such as $A=6$ and $A=12$, but has been problematic in the $A=14$ system, where the anomalously suppressed beta decay $^{14}\mathrm{C}_{\mathrm{g.s.}}\rightarrow {}^{14}\mathrm{N}_{\mathrm{g.s.}}+e^-+\bar{\nu}_e$ is not helpful to constrain the $^{14}\mathrm{C}_{\mathrm{g.s.}}$ and $^{14}\mathrm{N}_{\mathrm{g.s.}}$ wave functions [2,3]. Such an unusually small amplitude is certain to be influenced by the two-body effects such as meson exchange currents [4]. In the past two decades, the experimental database has improved considerably, with the availability of more precise and higher momentum transfer electron scattering data [3,5–13] from the improved electron facilities. These can provide crucial information about nuclear charge, current, and spin transition densities, often revealing regimes where new physics comes into play. Our objective is to systematically examine such observables as can be adequately described with one-body matrix elements and thus can be used as precise constraints on the nuclear wave functions.

At low momentum transfers, the nucleus can be described by nonrelativistic single-particle motions in a nuclear mean field. At higher momentum transfers, relativistic corrections and two-body effects such as meson exchange currents can play a significant role [14]. Electromagnetic and weak observables, such as static electric and magnetic moments, electron scattering form factors, β decay, and μ-capture amplitudes, can provide constraints for the nuclear structure at low momentum transfer $|\vec{q}|$ [1,3,5–10,15,16] . For β decay, $|\vec{q}|\approx 0.01\ \mathrm{fm}^{-1}$, and for muon capture, $|\vec{q}|\approx 0.7\ \mathrm{fm}^{-1}$. We restrict our study to the $1p$-shell nuclear transitions at low momentum transfer so that the two-body contributions will be small, or in specific cases, to regions of momentum transfer in which the two-body effects, such as meson exchange currents, have been explicitly calculated to be small. An exception to this will be the $A=14$ case: Here the nuclear structure conspires to make one-body electroweak amplitudes small, thereby enhancing the role of the two-body effects. Also, the inelastic transitions studied here are of pure $M1$ character, in order to reduce uncertainties due to two-body corrections that have a strong dependence on multipolarity.

In studying transitions between $^6\mathrm{Li}_{\mathrm{g.s.}}$ and $^6\mathrm{Li}^*$(3.56 MeV, $J^\pi T=0^+1$), one can gain information concerning the nuclear structure of $^6\mathrm{He}_{\mathrm{g.s.}}$, as the excited state is its isobaric analog. Similarly, the $^{14}\mathrm{N}^*$(2.313 MeV, $J^\pi T=0^+1$) level is the isobaric analog to $^{14}\mathrm{C}_{\mathrm{g.s.}}$ and the $^{12}\mathrm{C}^*$(15.11 MeV, $J^\pi T=1^+1$) state is the analog to $^{12}\mathrm{B}_{\mathrm{g.s.}}$. Thus, the nuclear structure information so gained can be applied to the photoproduction reactions $^6\mathrm{Li}_{\mathrm{g.s.}}$ $(\gamma,\pi^+)\,^6\mathrm{He}_{\mathrm{g.s.}}$, $^{12}\mathrm{C}_{\mathrm{g.s.}}$ $(\gamma,\pi^+)\,^{12}\mathrm{B}_{\mathrm{g.s.}}$, and $^{14}\mathrm{N}_{\mathrm{g.s.}}$ $(\gamma,\pi^+)\,^{14}\mathrm{C}_{\mathrm{g.s.}}$, assuming isospin invariance. We investigate these reactions in a paper with Wittman [17].

While the method of determining effective one-body amplitudes from the electroweak observables have been revisited many times since the work of Donnelly and Walecka, our strategy makes use of the powerful fitting procedures of the CERN fitter routine MINUIT. This allows us to explore the multidimensional parameter space in an exhaustive fashion not attempted previously for this problem. It allows us to distinguish among local minima in the multidimensional χ^2 space. We use this procedure with the latest electroweak database to explore the limits of the present method reachable with this data set.

II. PHENOMENOLOGICAL AMPLITUDES

We review the theoretical formalism in brief, to define quantities of interest to our analysis. In general, one can parametrize the phenomenological amplitudes in terms of doubly reduced transition density matrix elements (TDME's) [1]:

$$\Phi^{fi}_{\beta\alpha;JT}=\langle J^\pi_f T_f|||[a^\dagger_\beta\otimes S_{-\alpha}a_\alpha]^T_J|||J^\pi_i T_i\rangle/([J][T]),\quad (1)$$

where $a^\dagger_\beta$ is the particle creation operator with β labelling the single-particle quantum numbers $\{j_\beta m_\beta \tfrac{1}{2}\ \kappa_\beta\}$, $\tfrac{1}{2}$ is the

*Present address: University of Kentucky, Lexington, KY 40506.

nucleon isospin, κ is the isospin projection, and $[x]\equiv\sqrt{2x+1}$. The negative subscript denotes spin and isospin projections of opposite sign. J, π, and T are the nuclear angular momentum, parity, and isospin, respectively. The phase $S_{-\alpha}$ relates the single-hole creation operator $b^{\dagger}_{\alpha}$ to the single-particle destruction operator:

$$b^{\dagger}_{\alpha}=S_{\alpha}a_{-\alpha}=(-1)^{j_{\alpha}+m_{\alpha}+1/2+\kappa_{\alpha}}a_{-\alpha}, \tag{2}$$

where $b^{\dagger}_{\alpha}|0\rangle=|\alpha^{-1}\rangle$ and $\tilde{a}_{\alpha}$ annhilates the time reversed particle state $|\tilde{\alpha}\rangle$. The $b^{\dagger}_{\alpha}$ form the components of a spherical tensor operator of rank j_{α} [18].

The $\Phi^{fi}_{\beta\alpha;JT}$ are related to the $A_{(LS)J\ 1/2}$ of Lee and Kurath [19], where $\frac{1}{2}$ is the isospin projection, by

$$\Phi^{fi}_{\beta\alpha;JT}=\frac{(-1)^{T_f-T_i+1}[J_f][T_f]}{\sqrt{2}\langle T0T_i-T_i|T_f-T_i\rangle}[j_{\beta}][j_{\alpha}]\sum_{LS}[L][S]\begin{Bmatrix}1 & 1 & L\\ \frac{1}{2} & \frac{1}{2} & S\\ j_{\beta} & j_{\alpha} & J\end{Bmatrix}(A_{(LS)J\ 1/2}+(-1)^{T}A_{(LS)J-1/2}). \tag{3}$$

The TDME's are used to evaluate the nuclear matrix elements of one-body operators:

$$\langle J_fT_f|||F^{JT}|||J_iT_i\rangle=\sum_{j_{\beta}j_{\alpha}}\langle\beta|||f^{JT}|||\alpha\rangle\Phi^{fi}_{\beta\alpha;JT}, \tag{4}$$

The TDME's for nonscalar transitions involving hole states can be cast into the same form as the TDME's for transitions involving particle states [20]:

$$\langle J_fT_f|||F^{JT}|||J_iT_i\rangle=\sum_{j_{\beta}j_{\alpha}}\langle\beta|||f^{JT}_{c}|||\alpha\rangle\langle J_fT_f|||[b^{\dagger}_{\beta}\otimes S_{-\alpha}b_{\alpha}]^{JM}_{T\Lambda}|||J_iT_i\rangle/([J][T]), \tag{5}$$

where

$$f^{JT}_{c}\equiv-(\mathfrak{J}^{-1}f^{JT}\mathfrak{J})^{\dagger}=(-1)^{1+J+T}f,$$

and the time reversal operator $\mathfrak{J}=e^{i\pi(\sigma_2+\tau_2)/2}K$, where K is the complex conjugation operation and $\mathfrak{J}|\alpha\rangle=|\tilde{\alpha}\rangle$. TDME's defined in this way for the mass-6 and mass-14 cases have the same dependence on the wave function basis components. Thus, to obtain the nuclear matrix element of a one-body operator for transitions involving n-hole states, one need only multiply the corresponding nuclear matrix element for the n-particle case by the phase $(-1)^{1+J+T}$.

The wave functions for the $^{6}\mathrm{He}_{\mathrm{g.s.}}$, $^{6}\mathrm{Li}_{\mathrm{g.s.}}$ states $^{14}\mathrm{C}_{\mathrm{g.s.}}$, $^{14}\mathrm{N}_{\mathrm{g.s.}}$ and the aforementioned isobaric analog levels are explicitly constructed within the $1p$-shell basis. The ground state quantum numbers of ^{6}Li and ^{14}N are $J^{\pi}T=1^{+}0$; the ground state quantum numbers of ^{6}He and ^{14}C are $J^{\pi}T=0^{+}1$. The normalized wave functions in the jj representation are

$$|1^{+}0\rangle=\sum_{k_i}c_{k_i}|\phi^{\sigma}_{k_i}\rangle=a|p^{\sigma}_{1/2}p^{\sigma}_{1/2}\rangle+b|p^{\sigma}_{3/2}p^{\sigma}_{1/2}\rangle+c|p^{\sigma}_{3/2}p^{\sigma}_{3/2}\rangle,\quad |0^{+}1\rangle=\sum_{k_f}c_{k_f}|\phi^{\sigma}_{fk}\rangle=m|p^{\sigma}_{1/2}p^{\sigma}_{1/2}\rangle+n|p^{\sigma}_{3/2}p^{\sigma}_{3/2}\rangle, \tag{6}$$

where $\sigma=+1$ for $A=6$, -1 for $A=14$, representing particle and hole, respectively. The corresponding normalized wave functions in the LS representation are

$$|1^{+}0\rangle=\alpha|^{3}S_{1}\rangle+\beta|^{1}P_{1}\rangle+\gamma|^{3}D_{1}\rangle,\quad |0^{+}1\rangle=x|^{1}S_{0}\rangle+y|^{3}P_{0}\rangle. \tag{7}$$

The TDME's for elastic transitions are constrained by the fact that the ground state wave function is an eigenstate of total angular momentum $\vec{J}=\Sigma_i\vec{j}_i$ so that [21]

$$\langle 1^{+}0|||\vec{J}|||1^{+}0\rangle=\sqrt{6}=\sum_{\beta\alpha}\langle\beta|||\vec{j}|||\alpha\rangle\Phi^{ii}_{\beta\alpha;10}=\sqrt{2}\sum_{\alpha}[j_{\alpha}]\sqrt{j_{\alpha}(j_{\alpha}+1)}\Phi^{ii}_{\alpha\alpha;10}. \tag{8}$$

In addition, time reversal invariance imposes the constraint

$$\Phi^{ii}_{\beta\alpha;J0}=(-1)^{j_{\alpha}+j_{\beta}}\Phi^{ii}_{\alpha\beta;J0}(\alpha\neq\beta). \tag{9}$$

Thus, only two of the four $1p$-shell elastic TDME's are independent. The normalized $^{6}\mathrm{Li}_{\mathrm{g.s.}}$ and $^{14}\mathrm{N}_{\mathrm{g.s.}}$ $1p$-shell wave functions in Eq. (6) also have two independent parameters, so that Eqs. (8) and (9) do not impose additional constraints. Note that there are no constraints on the $1p$-shell inelastic $J=1$, $T=1$ TDME's, independent of reference to a wave function basis. However, the normalized excited state wave function in Eq. (6) is a function of just one independent parameter, implying that there is only one independent inelastic TDME for the mass-6 and mass-14 cases. It is pos-

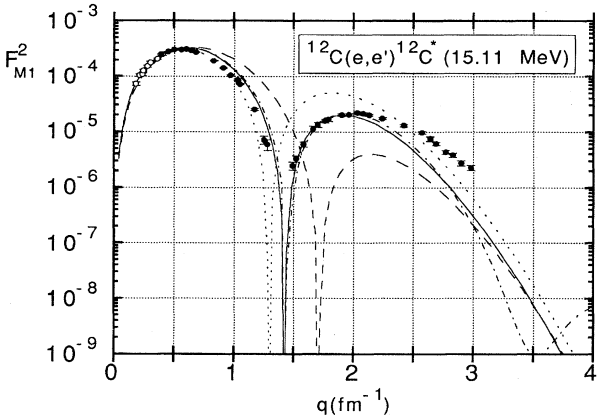

FIG. 1. ^{12}C 15.11 MeV $M1$ (e,e') form factor: RPI-C2 (solid curve), Cohen-Kurath (long-dashed curve), RPI-C1 (dotted curve), and RPI-C2 with HF radial wave functions (dash-dot curve). The data are from Ref. [11] (open circles) and Ref. [12] (solid circles).

sible that this additional freedom can appear as the renormalization of the TDME's. Specifically, we examine the possible renormalization of the $\Phi_{LS;JT} = \Phi_{21;11}$ matrix element, presumably due to s-d shell admixtures [22].

We do not explicitly construct a $1p$-shell wave function for $^{12}C_{g.s.}$. Instead we use the TDME's to compute the off-diagonal observables between $^{12}C_{g.s.}$ and the $^{12}C^*(15.11$ MeV, $J^\pi T = 1^+1)$ level, the isobaric analog of $^{12}B_{g.s.}$. These TDME's are, in the notation of Eq. (1), $\Phi_{1/2\;1/2\;;11}$, $\Phi_{1/2\;3/2\;;11} - \Phi_{3/2\;1/2\;;11}$, and $\Phi_{3/2\;3/2\;;11}$. Note that $\Phi_{1/2\;3/2\;;11}$ and $\Phi_{3/2\;1/2\;;11}$ cannot be fit separately since the relevant $T=1$ observables are a function of their difference. In the jj-coupling limit $^{12}C_{g.s.}$ is a closed $p_{3/2}$ subshell and the 15.11 MeV level is a $p_{3/2}$-hole–$p_{1/2}$-particle state, $\Phi_{1/2\;1/2\;;11} = \Phi_{3/2\;3/2\;;11} = \Phi_{3/2\;1/2\;;11} = 0$, and $\Phi_{1/2\;3/2\;;11} = 1$. However, the jj limit gives a poor representation of the nuclear structure [23]. We use Eq. (4) to evaluate the nuclear matrix elements for the mass-12 case with the single-body matrix element evaluated for particle states, since, for example, the mass-12 wave functions can be regarded as eight $1p$-shell particles on the ^{4}He core.

For the radial wave functions we use harmonic oscillator (HO) as well as Hartree-Fock (HF) functions [24], based on the Skyrme interaction, for $^{12}C_{g.s.}$ and $^{14}N_{g.s.}$. An additional degree of freedom is introduced in the HO case: The $p_{1/2}$ and $p_{3/2}$ radial functions have their own *effective* oscillator parameters $b_{1/2}$ and $b_{3/2}$, in order to simulate the effect of the spin-orbit splitting. The effectiveness of this parametrization can be tested by comparing observables calculated using the realistic Hartree-Fock wave functions with those calculated using HO functions that maximize the overlap integral with the $p_{1/2}$ and $p_{3/2}$ HF radial functions, as used in Ref. [24]. This procedure yields $b_{1/2}$ = 1.80 fm and $b_{3/2}$ = 1.64 fm. Evaluating the difference in HO energies between the $p_{1/2}$ and $p_{3/2}$ states yields

$$\Delta E = \frac{5}{2}\frac{\hbar^2}{M}\left(\frac{1}{b_{3/2}^2} - \frac{1}{b_{1/2}^2}\right) = 6.6 \text{ MeV}, \tag{10}$$

TABLE I. $C_{\beta\alpha\ell}$ of Eq. (11).

$\beta\alpha$	$C^{\rm spin}_{\beta\alpha 0}$	$C^{\rm orb}_{\beta\alpha 0}$	$C^{\rm spin}_{\beta\alpha 2}$	$C^{\rm orb}_{\beta\alpha 2}$
$\frac{1}{2}\frac{1}{2}$	$-\frac{1}{2\sqrt{2}}$	$\frac{1}{\sqrt{2}}$	$\frac{1}{2}$	$\frac{1}{2}$
$\frac{1}{2}\frac{3}{2}$	1	$-\frac{1}{2}$	$\frac{1}{4}$	$-\frac{1}{2}$
$\frac{3}{2}\frac{3}{2}$	$\frac{\sqrt{5}}{2}$	$\frac{\sqrt{5}}{2}$	$-\frac{1}{2\sqrt{5}}$	$\frac{\sqrt{5}}{2}$

consistent with the observed spin-orbit splitting in the $1p$-shell nuclei [24].

In Fig. 1 we show the ^{12}C 15.11 MeV (e,e') form factor using the HF and "effective" HO radial wave functions and the same nuclear structure information (RPI-C2, to be discussed shortly). The two radial inputs give nearly identical results out to momentum transfer $q = 2.9$ fm^{-1}. The HF radial input shows an additional diffraction structure whereas the HO result decays monotonically at higher q. Thus, we conclude that the "effective" HO radial wave functions can be used to simulate the behavior of realistic radial wave functions at momentum transfers less than 3.0 fm^{-1}.

III. ELECTROMAGNETIC AND WEAK INTERACTION OBSERVABLES

We now test the contention [1] that electroweak observables can be described in the chosen nuclear transitions in an approach in which the two-body effects are ignored, and possibly absorbed by the phenomenological amplitude. Two-body corrections are, in general, observable dependent, and our procedure would fail to absorb them in the effective one-body amplitudes in a fit, where two-body corrections to different observables are significantly different. For example, if the two-body corrections to the electromagnetic current are strongly isospin dependent, the elastic $T = 0$ and inelastic $T = 1$ (e,e') form factors will not be simultaneously described and other observables will have to be explored as possible constraints for the wave function. Also, since the corrections to the (e,e') form factors are dependent on momentum transfer, only specific ranges of momentum transfer may be useful for extracting the phenomenological amplitude. We can test this supposition by performing successive fits in which an additional (e,e') form factor data point outside a given range is included. Given precise and accurate data, the fits can signal the breakdown of the underlying nuclear model configuration space and thus characterize the region of validity in momentum transfer for a given model space.

A. Electromagnetic form factors

Evaluating the $M1$ form factor with $1p$-shell basis functions yields

$$F_T^{M1}(q)=\frac{2q[T]f_{sn}(q)}{3[T_f][J_i]ZM}\sum_{\alpha\beta\ell} F_{\text{c.m.}}^{\beta\alpha}(q)(C_{\beta\alpha\ell}^{\text{orb}}+\mu_T C_{\beta\alpha\ell}^{\text{spin}})\Phi_{\beta\alpha;1T}^{fi}B_\ell^{\beta\alpha}(q), \tag{11}$$

where

$$B_\ell^{\beta\alpha}(q)=\langle R_\beta|j_\ell(qr)|R_\alpha\rangle,$$

and $\ell=\{0,2\}$, $T=\{0,1\}$, and $\mu_T=\mu_p+(-1)^T\mu_n$. Hence, $\mu_0=0.879\,804$ and $\mu_1=4.705\,888$ nuclear magnetons [25]. The $C_{\beta\alpha\ell}$ are given in Table I (where $C_{3/2\ 1/2\ell}=-C_{1/2\ 3/2\ell}$). $f_{sn}(q)$ is the nucleon size correction:

$$f_{sn}(q)=1/(1+q^2/18.43\ \text{fm}^{-2})^2. \tag{12}$$

$F_{\text{c.m.}}^{\beta\alpha}(q)$ is the center-of-mass (c.m.) correction factor. For $p_{1/2}$ and $p_{3/2}$ harmonic oscillator wave functions, the Bessel transforms are

$$B_0^{\beta\alpha}(y)=\left(1-\frac{2y_{\beta\alpha}}{3}\right)N_{\beta\alpha}e^{-y_{\beta\alpha}},\quad B_2^{\beta\alpha}(y)=\frac{2}{3}N_{\beta\alpha}e^{-y_{\beta\alpha}}, \tag{13}$$

where

$$y_{\beta\alpha}=\frac{q^2b_{\beta\alpha}^2}{4},\quad b_{\beta\alpha}^2=\frac{2b_\beta^2b_\alpha^2}{b_\beta^2+b_\alpha^2},\quad \text{and}\quad N_{1/2\ 3/2}=\left[\frac{b_{1/2\ 3/2}}{\sqrt{\{b_{1/2}b_{3/2}\}}}\right]^5.$$

For the effective harmonic oscillator functions, the normalization factor $N_{1/2\ 3/2}=0.989$. Numerically evaluating $N_{1/2\ 3/2}$ in the HF case gives $N_{1/2\ 3/2}=0.990$.

In some Hartree-Fock approaches [24,26], the c.m. correction is obtained by subtracting the total c.m. kinetic energy $\vec{P}^2/2MA$ from the sum of the single-particle kinetic energies $\Sigma_i\vec{p}_i^{\,2}/2M$, where M is the nucleon mass and A is the nuclear mass number. This procedure effectively reduces the single-particle kinetic energy by a factor of $(1-1/A)$ and introduces correlation terms of the type $\vec{p}_i\cdot\vec{p}_j$. Applying this correction improves the agreement of the calculated single-particle energies with their experimental values even when these correlations are ignored [26]. Campi and Sprung [27] found that including the correlations introduces technical difficulties. As in this work, they opted to use the c.m. correction appropriate for harmonic oscillator functions, where the harmonic oscillator functions are determined from maximum overlap with the HF functions. This yields $F_{\text{c.m.}}^{\beta\alpha}(y)=e^{y_{\beta\alpha}/A}$.

B. Ground state moments

The single-particle magnetic moment operator is given by [28]

$$\vec{\mu}=\tau_p\vec{L}+\frac{1}{2}(\mu_0-\mu_1\tau_3)\vec{\sigma}. \tag{14}$$

The nuclear matrix element of μ_z yields, in nuclear magnetons,

$$\mu\equiv\langle 1^+0|\mu_z|1^+0\rangle=\frac{\sqrt{2}}{3}\left[(1-\mu_0/2)\Phi_{1/2\ 1/2\ ;10}+2\sqrt{2}N_{1/2\ 3/2}\left(\frac{1}{2}-\mu_0\right)\Phi_{1/2\ 3/2\ ;10}+\sqrt{\frac{5}{2}}(1+\mu_0)\Phi_{3/2\ 3/2\ ;10}\right]. \tag{15}$$

The single-particle quadrupole moment operator is [28]

$$Q_{op}=\sqrt{\frac{16\pi}{5}}er^2Y_{20}\tau_p. \tag{16}$$

The nuclear matrix element of Q is

$$Q\equiv\langle 1^+0|Q_{op}|1^+0\rangle=\frac{4e}{5\sqrt{5}}\left(N_{1/2\ 3/2}\langle R_{1/2}|r^2|R_{3/2}\rangle\Phi_{1/2\ 3/2\ ;20}-\frac{1}{2}\langle R_{3/2}|r^2|R_{3/2}\rangle\Phi_{3/2\ 3/2\ ;20}\right). \tag{17}$$

For harmonic oscillator radial wave functions,

$$\langle R_\beta|r^2|R_\alpha\rangle=\frac{5}{2}\frac{b_{\beta\alpha}^7}{(b_\beta b_\alpha)^{5/2}}. \tag{18}$$

TABLE II. ^{12}C phenomenological amplitudes, observables, and χ^2_ν.

	$\Phi_{1/2\ 1/2\ ;11}$	$\Delta\Phi_{;11}$	$\Phi_{3/2\ 3/2\ ;11}$	$b_{1/2}$ (fm)	$b_{3/2}$ (fm)	ft (10^4 sec)	T_γ^{M1} (asec)	χ^2_ν
RPI-C1	0.183	-0.142	-0.209	1.80	1.64	1.17	17.6	1.2
RPI-C2	0.0781	-0.380	-0.0655	1.80	1.64	0.989	18.0	1.1
CK	0.0578	0.351	0.0765	1.65	1.65	1.24	21.3	200
Haxton [15]	0.111	-0.338	-0.0865	1.757	1.757	1.00	18.0	2.1
ODW [16]	0	0.444	0	1.77	1.77	1.14	22.2	36
j-j limit	0	1	0	1.65	1.65	0.225	4.4	10^5

C. $M1$ radiative lifetime

The $M1$ radiative lifetime provides an additional constraint to the inelastic (e,e') form factor at zero momentum transfer:

$$T_\gamma^{M1}=\frac{[J_i]^2[T_f]^2}{2e^2E^3\langle T_i\Lambda_i 1-1|T_f\Lambda_f\rangle^2\langle|J_fT_f|||F_1^{M1}(0)|||J_iT_i\rangle|^2}\,, \tag{19}$$

where E is the excitation energy.

D. Nuclear beta decay

The nuclear β-decay ft value is given by

$$ft_\beta=\frac{4h\pi^3[J_i]^2[T_i]^2}{g_a^2G_\beta^2m^5\langle T_i\Lambda_i 1-1|T_f\Lambda_f\rangle^2|\langle J_fT_f|||\vec{\sigma}\vec{\tau}|||J_iT_i\rangle|^2}\,, \tag{20}$$

where

$$\langle J_fT_f|||\vec{\sigma}\vec{\tau}|||J_iT_i\rangle=\frac{2}{3}[-\Phi_{1/2\ 1/2\ ;11}+2\sqrt{2}N_{1/2\ 3/2}(\Phi_{1/2\ 3/2\ ;11}-\Phi_{3/2\ 1/2\ ;11})+\sqrt{10}\Phi_{3/2\ 3/2\ ;11}]$$

and m is the electron mass; we use $g_A=1.254$ and $G_\beta=1.13602\times10^{-5}$ GeV^{-2} [29].

IV. FITS

We seek to refine the χ^2 function minimization analysis, presenting additional fit strategies unexplored by other authors, such as the sensitivity of the fitting procedure to (1) different starting points in the χ^2 space, (2) various ranges of momentum transfer $q=|\vec{q}|$ in the (e,e') form factor data, in order to establish a q region of validity of the underlying model, and (3) different parametrizations of the model, in order to minimize the correlations between the parameter errors. In regard to item (1), physically motivated starting points are used, such as the ones expected in a $1p$-shell model, or ones that arise from constraining the parameters with experimental information. In regard to item (2), we do not wish to include q regions in the (e,e') form factors that are significantly effected by meson exchange currents. We use the MINUIT [30] release (90.10) from the CERN program library.

For the case of many local minima, there is no guarantee that the global minimum will be found. However, the fit can be guided to physically meaningful minima by using starting points $\vec{a}$ deduced from experimental constraints. For example, given the wave function parametrizations for the mass-6 and -14 cases in Eqs. (6) and (7), we can use any three of the four observables μ, Q, T_γ, and ft_β, to obtain the $\vec{a}$. Also, Cohen-Kurath (CK) [31] TDME's may serve as useful starting points. The CK amplitudes are derived from fits of matrix elements of the two-body interaction to energy differences between the ground and low-lying excited states of regular parity throughout the $1p$ shell.

V. RESULTS

A. ^{12}C

We fit the 15.11 MeV $M1$ (e,e') form factor, the $^{12}B_{g.s.}\rightarrow{}^{12}C_{g.s.}$ β-decay ft value, and the T_γ^{M1} of $^{12}C^*(15.11$ MeV, $J^\pi T=1^+1)\rightarrow{}^{12}C_{g.s.}$. HF radial wave functions are used for the $p_{3/2}$ and $p_{1/2}$ states. The chi-squared per degree of freedom χ^2_ν increases from 1.1 to 3.0 when the (e,e') data point at $q=1.03$ fm^{-1} is included along with the lower momentum transfer data. This q value serves as the momentum transfer cutoff for this fit. This fit, denoted RPI-C1, is given in Table II, where $\Delta\Phi_{;11}\equiv\Phi_{1/2\ 3/2\ ;11}-\Phi_{3/2\ 1/2\ ;11}$. The experimental values of ft_β and T_γ^{M1} are 11 668±23 sec and 17.8±0.5 asec, respectively [32]. The oscillator parameters used with the Cohen-Kurath [19,31] amplitudes are deduced from the rms radius of the charge distribution [33]. χ^2_ν is calculated for the

TABLE III. ^{6}Li algebraic solutions.

	α	β	γ	x	y	Prediction	Experiment [38]
A1$^+$	0.923	0.371	0.099	0.997	0.072	T_γ^{M1} = 86 asec	81.0$\pm$1.6 asec
A1$^-$	0.923	-0.371	0.099	0.864	0.503	T_γ^{M1} = 121 asec	
A2$^+$	0.923	0.371	0.099	0.864	-0.503	T_γ^{M1} = 79.1 asec	
A2$^-$	0.923	-0.371	0.099	0.997	-0.072	T_γ^{M1} = 111 asec	
B1$^+$	0.923	0.371	0.099	1.000	-0.009	ft_β=778 sec	813$\pm$16 sec
B2$^+$	0.923	0.371	0.099	0.841	-0.541	ft_β=837 sec	
C2$^+$	0.964	0.326	0.175	0.878	-0.479	$Q=-4.2$ mb	-0.644 ± 0.007 mb
D1$^+$	0.883	0.447	0.139	0.994	-0.105	$\mu=0.793\ \mu_N$	$0.82205\pm10^{-5}\ \mu_N$
D2$^+$	0.964	0.260	0.057	0.860	-0.510	$\mu=0.852\ \mu_N$	

amplitudes other than RPI-C1 and RPI-C2 in Table II using the form factor points fit by RPI-C1.

The $M1$ (e,e') form factor, obtained using the RPI-C1 amplitudes as input, is shown in Fig. 1. The computed form factor is in good agreement with the low momentum transfer data, but in strong disagreement with the data at the second maximum of the form factor. This is not surprising in view of the 30% meson exchange current (MEC) contribution in the region of the first maximum as estimated by Dubach and Haxton (DH) [34]. However, DH found that the MEC contributions to the second maximum are small. With this in mind, we fit the one-body density to the (e,e') data at the second maximum and below $q=0.5$ fm^{-1}. This procedure yields fit RPI-C2 (Table II). Its prediction for the $M1$ (e,e') form factor is shown in Fig. 1. T_γ^{M1} is also included in the fit, whereas ft_β is not. ft_β deviates from the experimental value by about 15%. In the L-S coupling, the TDME's for the Haxton amplitude and RPI-C2 are nearly identical except for the $\Phi_{LS;JT}=\Phi_{21;11}$ amplitude (-0.016 vs 0.029). This is due to our insistence on fitting the second lobe of the form factor, ignoring the q^2 region where MEC contributes, and on our fit to more recent (e,e') data.

We conclude that the amplitude RPI-C2 is a good determination of the $1p$-shell one-body transition density up to $q\approx2.0$ fm^{-1} and thus should serve as a reliable input to our $^{12}C_{g.s.}$ (γ,π^+) $^{12}B_{g.s.}$ calculation at low energy. At higher q, nuclear excitations to higher shells are clearly needed [35].

B. ^{6}Li

1. Algebraic solutions

There are three independent basis components describing $^6Li_{g.s.}$ and ^{6}Li*(3.56 MeV, $J^\pi T=0^+1$), given the normalized phenomenological amplitude (PA) of Eq. (7). Thus, any three of the four observables μ, Q, T_γ^{M1} and ft_β, can be used to constrain the c_i. These c_i are nearly independent of the radial wave function, since the observables are evaluated at close to zero momentum transfer. Note that we use an earlier experimental value for Q (-0.644 mb) [36]. The PA change negligibly when the latest Q value (-0.83 mb) [37] is used: Fine differences in the $1p$-shell basis reproduce the small ^{6}Li Q value.

A weak radial dependence enters in the cases where Q is used as a constraint, due to its proportionality to the p-shell rms radius (PRMS). Since the algebraic solutions are used simply as a guide to the full fits, an estimate of the PRMS is deduced from a one-oscillator parameter fit to the elastic and inelastic form factor data up to $q_{\max}^{\Delta T=0}=1.76$ fm^{-1} and $q_{\max}^{\Delta T=1}=1.03$ fm^{-1}, respectively. This yields $b_{1/2}$ = $b_{3/2}$ = 2.0 fm and PRMS = 3.16 fm. Including q points in the fits above the $q_{\max}$ leads to a sharp rise in χ^2_ν.

The quadratic dependence of the observables on the PA leads to two branches of solution, denoted 1 and 2. We are free to choose the phase of the $|^1P_1\rangle$ state (denoted by the superscript $\pm$), and so have a total of 16 possible solutions, not all of which exist. The sets of observables used to find the solutions are labeled by A for (μ,Q, and ft_β), B for (μ,Q, and T_γ^{M1}), C for (μ, T_γ^{M1} and ft_β), and D for (Q, T_γ^{M1}, and ft_β) (see Table III). The branches of solution that are close to the $|p_{3/2}p_{3/2}\rangle$ limit for $^6He_{g.s.}$ ($x=0.816$ and $y=-0.577$) are not physically acceptable due to the weakness of the spin-orbit interaction in ^{6}Li. The B1$^+$ and B2$^+$ solutions are nearly identical to the SASK-B and SASK-A amplitudes of Ref. [6]. We calculate the value of the fourth unconstrained observable in Table III and compare to the experimental values. Of the $|^1S_0\rangle$-type solutions, the A1$^+$, B1$^+$, and D1$^+$ predictions come closest to experiment. This algebraic exercise illustrates the possibility of many local minima in the χ^2 space, due to the nonlinear dependence of the observables on the PA. We presently use the form factor to choose the optimal solution.

2. Fits

With the A1$^+$ solution as a starting point, and fitting the observables that constrained this solution, we obtain the fit RPI-L (Table IV), with $q_{\max}^{\Delta T=1}=1.76$ fm^{-1} and $q_{\max}^{\Delta T=1}=1.03$ fm^{-1}. The fits corresponding to the B1$^+$ and D1$^+$ starting points have parameters similar to RPI-L, but about a 50% larger χ^2_ν. As an example of the starting point dependence of the fits, we use the $\alpha=x=1$ limit, rather than the A1$^+$ solu-

TABLE IV. $A=6$ phenomenological amplitudes.

	α	β	γ	x	y	$b_{1/2}$ (fm)	$b_{3/2}$ (fm)
RPI-L	0.928	0.366	0.071	0.996	0.094	2.30	1.93
RPI-SHO	0.902	0.415	0.120	0.996	0.084	2.01	2.01
STAN-HO [1]	0.924	0.369	0.102	1.00	0.028	2.03	2.03
CK [19,31]	0.958	0.076	0.276	1.00	-0.024	1.98	1.98
SASK-A [6]	0.924	0.369	0.101	0.844	-0.537	1.80	1.80
SASK-B [6]	0.924	0.369	0.100	1.00	-0.010	1.85	1.85

TABLE V. $A=6$ phenomenological amplitudes: observables and χ_ν^2.

	μ (μ_N)	Q (mb)	ft (sec)	T_γ^{M1} (asec)	χ_ν^2
Expt [38].	0.82205	-0.644	813±16	81.0±1.6	
RPI-L	0.826	-0.644	847	89.1	1.8
RPI-SHO	0.806	-0.644	864	89.2	2.8
STAN-HO [1]	0.822	-0.815	792	82.9	10.
CK [19,31]	0.833	-10.2	688	83.9	37.
SASK-A [6]	0.822	-0.8	835	80.9	400
SASK-B [6]	0.822	-0.8	777	80.9	300
$\alpha=x=1$	0.880	0	667	79.5	22

tion as a starting point. This yields a fit similar to RPI-L, except that the excited state has $n\approx1$. The "effective" spin-orbit energy for RPI-L is 8.2 MeV as calculated via Eq. (10). This is higher than the value one would expect near the beginning of the $1p$ shell and may indicate the unbound nature of the $p_{1/2}$ orbital. The amplitude STAN-HO [1] fits an older (e,e') database. Our amplitude RPI-SHO fits the same observables as in the STAN-HO fit, namely, μ, Q, and the (e,e') form factors, with $b_{1/2} = b_{3/2}$ and the same $q_{\max}$ used for RPI-L. χ_ν^2 is calculated for the amplitudes other than RPI-L and RPI-SHO in Table V using the form factor points fit by RPI-L.

The large chi-squared obtained for the SASK-A and -B amplitudes corroborates the poor result found for the B1+ and B2+ branches of solution. The "one-branch" of the A solution is clearly favored by the fits. Thus, with foreknowledge of the possible solutions as starting points, we are able to specify the possible local minima in this case.

Static observables are calculated for the various PA in Table V. Note that the prediction for ft_β given by the amplitude RPI-L differs from the experimental value [38] by 4%, and contributes about 10% to χ_ν^2. Including meson exchange current corrections to the weak axial current responsible for the β decay brings the ft_β value to within 1% of the experimental value [20]. Thus we conclude that the amplitude RPI-L gives a good prediction for the $\Phi_{LS;JT}=\Phi_{01;11}$ one-body transition density matrix element.

The small ^{6}Li Q is well reproduced in the $1p$-shell basis, indicating that polarization of the ^{4}He core is not important here. The first 2^+ level in ^{4}He occurs at about 25 MeV excitation. In contrast, the first 2^+ level occurs at 6.9 MeV [39] in ^{16}O, so that the core polarization effects should be of greater importance in the ^{14}N case.

The elastic and inelastic form factors are shown in Figs. 2 and 3, respectively. The SASK-B result is shown for their harmonic oscillator fit. We emphasize that our objective here is to fit the low-q data, where our model should be able to reproduce the gross features of the nuclear structure. Given the quality of the fit RPI-L, we feel our amplitude provides a good determination of the nuclear one-body transition density, and thus should be consistent with the low-energy pion photoproduction data in the corresponding momentum transfer range.

The cluster model [40] successfully predicts the inelastic $M1$ form factor throughout the momentum transfer range given by the experimental data. However, it has similar difficulties in reproducing the high-q region of the elastic $M1$

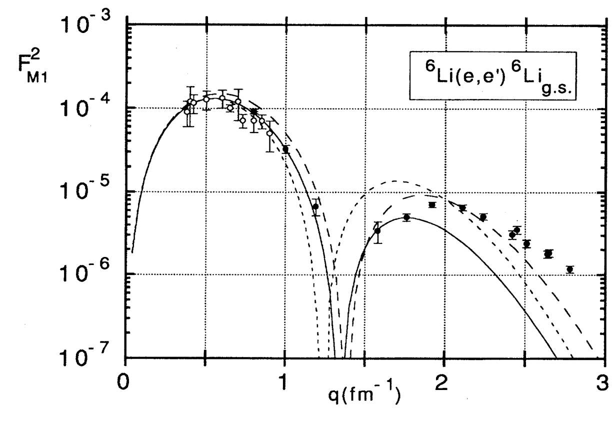

FIG. 2. ^{6}Li elastic $M1$ (e,e') form factor: RPI-L (solid curve), SASK-B (long-dashed curve), and Cohen-Kurath (short-dashed curve). The data are from Ref. [13] (open circles) and Ref. [7] (solid circles).

form factor. Note that we successfully reproduce the ^{6}He to ^{6}Li β-decay ft value when the meson exchange current contributions are taken into account. Also, Q is consistent with the $1p$-shell model whereas its prediction within the cluster model has met with difficulty. We emphasize, however, that we are mainly interested in consistency of observables at low q within a model that can be readily used for realistic medium energy calculations.

C. ^{14}N

1. Algebraic Solutions

The solutions to the experimental constraints [41] for the mass-14 case are given in Table VI. Unlike the mass-6 case, the two branches of solution are nearly degenerate. No satisfactory prediction of the fourth unconstrained observable is found. This is probably due to the fact that at least two of the observables are subject to significant two-body effects, such as core polarization, in the case of the quadrupole moment,

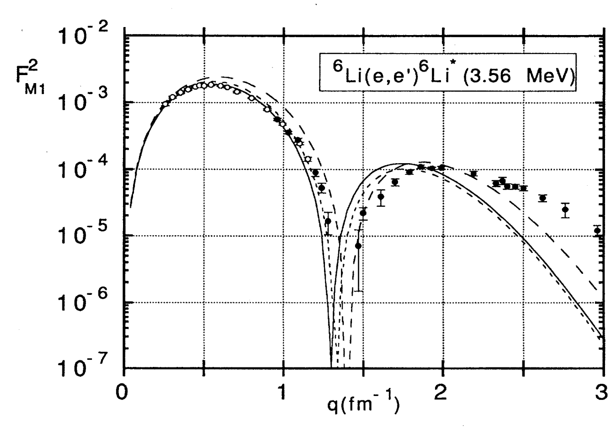

FIG. 3. ^{6}Li 3.56 MeV $M1$ (e,e') form factor: RPI-L (solid curve), SASK-B (long-dashed curve), and Cohen-Kurath (short-dashed curve). The data are from Ref. [8] (open circles) and Ref. [6] (solid circles).

TABLE VI. ^{14}N algebraic solutions.

	a	b	c	m	n	Prediction	Experiment [41]
A^-	0.551	-0.801	-0.233	-0.501	0.865	T_γ^{M1} = 49.4 fsec	92± 10 fsec
B^+	0.826	-0.526	0.202	0.972	-0.235	$ft_\beta = 1.65\times 10^7$ sec	1.1×10^9 sec
B^-	0.551	-0.801	-0.233	-0.455	0.891	$ft_\beta = 1.35\times 10^6$ sec	
C^+	0.991	0.085	-0.107	-0.295	0.956	$Q=-2.53$ mb	15.6 mb
C^-	0.587	-0.318	-0.745	0.999	0.039	$Q=-2.54$ mb	
D^+	0.739	-0.574	0.352	0.969	-0.247	$\mu=0.852\ \mu_N$	0.40376 μ_N
D^-	0.419	-0.895	-0.155	-0.558	0.830	$\mu=0.852\ \mu_N$	

or meson exchange currents, for example, in the case of the anomalously suppressed β-decay of $^{14}C_{g.s.}$ to $^{14}N_{g.s.}$.

2. Fits

For ^{14}N, we attempt to find an amplitude that is consistent with the strength of the spin-orbit coupling at the end of the $1p$ shell, i.e., where dominant component is $|p_{1/2}p_{1/2}\rangle$, such as for the Cohen-Kurath (CK) amplitudes. Other authors [5] have found the amplitude $H1$, which has $|p_{1/2}p_{1/2}\rangle$ as the dominant configuration in the ground state, but whose excited state is near the $|^3P_0\rangle$ limit. $H1$ is a fit of the phenomenological amplitude (PA) of Eq. (7) to the $^{14}N_{g.s.}$ elastic $M1$ (e,e') form factor, the $^{14}N_{g.s.}$ (e,e') ^{14}N*(2.313 MeV, $J^\pi T=0^+1$) form factor, μ, and T_γ^{M1}. Also, $H1$ has an unreasonably large value of the symmetry violating matrix element [22]. We have found an amplitude [42], denoted RPI-N1, which fits T_γ^{M1} and the inelastic form factor up to 1.7 fm^{-1} of momentum transfer (Table VII). RPI-N1 has $|p_{1/2}p_{1/2}\rangle$ as the dominant configuration in the excited state. However, this amplitude has a nearly $|^1P_1\rangle$ ground state and yields a poor description of the elastic observables. We were unable to find an amplitude that simultaneously fit the elastic and inelastic form factors, and which also yields an amplitude approximate to the Cohen-Kurath one, within the given parametrization. μ, Q, ft, and T_γ^{M1} are calculated for the various PA in Table VIII.

Amos, Koetsier, and Kurath (AKK) [22] recently undertook a reexamination of the mass-14 structure, pointing out that the CK amplitudes could be made consistent with the (e,e') form factors by introducing a 50% renormalization of the $\Phi_{LS;JT}=\Phi_{21;11}$ transition density, presumably due to core polarization effects. They found that this 50% renormalization of $\Phi_{21;11}$ is consistent with the $^{14}N_{g.s.}$ (p,p') ^{14}N* (2.313 MeV, $J^\pi T=0^+1$) and $^{14}C_{g.s.}$ (p,n) $^{14}N_{g.s.}$ reactions at 122 and 160 MeV. In addition, they found that the $B(M1)$ value for the ^{14}C*(11.31 MeV, $J^\pi T=1^+1)\rightarrow {}^{14}C_{g.s.}$ $(J^\pi T=0^+1)$ transition calculated using the CK amplitude is in better agreement with experiment than the value found using the amplitude $H1$.

TABLE VII. A = 14 phenomenological amplitudes.

	a	b	c	m	n	$b_{1/2}$	$b_{3/2}$
RPI-N1	0.519	0.104	0.848	0.957	0.291	1.62	1.51
RPI-N2	0.924	-0.268	0.200	0.968	0.250	1.69	1.69
H1 [5]	0.978	0.071	-0.196	0.553	-0.833	1.70	1.70
CK [19,31]	0.975	-0.207	-0.081	0.915	0.404	1.73	1.73
ENS [3]	0.676	-0.735	-0.053	0.759	-0.651	1.68	1.68

There has been considerable success in reproducing the $^{14}N_{g.s.}$ (γ,π^+) $^{14}C_{g.s.}$ data [43,44] at E_γ = 173, 200, 230, and 260 MeV using the amplitude $H1$ for the nuclear structure input [44,45]. The $\Phi_{21;11}$ transition density for $H1$ has a value of 0.433, which is about one-half the CK value of 0.827 [46]. Thus, the core polarization has been effectively absorbed into the $H1$ amplitude. However, the renormalized value of $\Phi_{21;11}$ should not be determined from the $1p$-shell wave function parameters, as was done with the $H1$ amplitude, since the corrections to the transition density extend to other shells. It is clear that the "true" renormalization of $\Phi_{21;11}$ cannot be obtained by our method, since we are using the $1p$-shell single-particle reduced matrix elements in the fits. Thus we fix $\Phi_{21;11}$ at one-half the CK value: $\Phi_{21;11}^{\rm AKK}=0.414$, and determine its unrenormalized value from the wave function parameters deduced from the other, presumably unrenormalized, TDME's. This defines a renormalization factor R_{21}:

$$R_{21}=\frac{\Phi_{21;11}^{\rm AKK}}{\Phi_{21;11}(\alpha,\beta,x)}\ . \tag{21}$$

Specifically, α and β are determined from the solutions to a quartic equation with $\Phi_{1/2\ 1/2\ ;10}$ and $\Phi_{1/2\ 3/2\ ;10}$ as inputs. x is found from the solutions to a quadratic equation as a function of either $\Phi_{01;11}$, and $\Phi_{10;11}$. This is another example of the inherent nonlinearity of our problem, which leads to many local minima in the χ^2 space.

Fitting the elastic form factor up to $q_{\rm max}^{\Delta T=0}=2.4$ fm^{-1}, the inelastic form factor up to $q_{\rm max}^{\Delta T=1}=1.7$ fm^{-1}, and T_γ^{M1}, the fit RPI-N2 is obtained with $\chi_\nu^2=1.3$ and $R_{21}=0.50$. This value of R_{21} is *precisely the one given in the AKK analysis*. The elastic and inelastic form factors are shown in Figs. 4 and 5, respectively. With the 50% renormalization of the Cohen-

TABLE VIII. $A=14$ phenomenological amplitudes: observables.

	μ (μ_N)	Q (mb)	ft (sec)	T_γ^{M1} (fsec)
Expt [41].	0.40376	15.6	1.1×10^9	92± 10
RPI-N1	0.537	-8.5	1.7×10^5	93.1
RPI-N2	0.364	7.80	1.7×10^5	102
H1 [5]	0.408	-2.29	2.1×10^5	140
CK [19,31]	0.331	5.93	2.61×10^4	107
ENS [3]	0.404	17.4	1.1×10^9	76.5
$a=m=1$	0.373	0	5.69×10^3	7.9

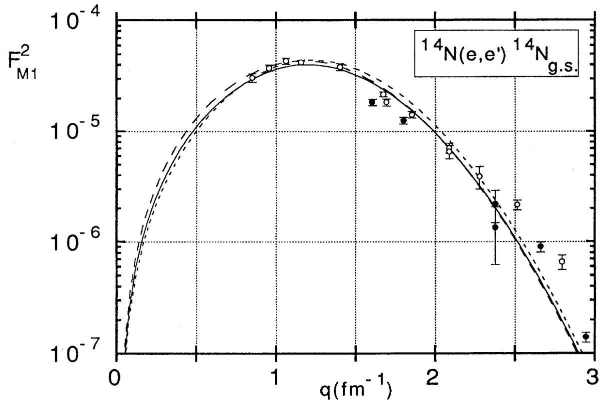

FIG. 4. ^{14}N elastic $M1$ (e,e') form factor: RPI-N2 (solid curve), $H1$ (long-dashed curve), and Cohen-Kurath (short-dashed curve). The data are from Ref. [5] (open circles) and Ref. [9] (solid circles).

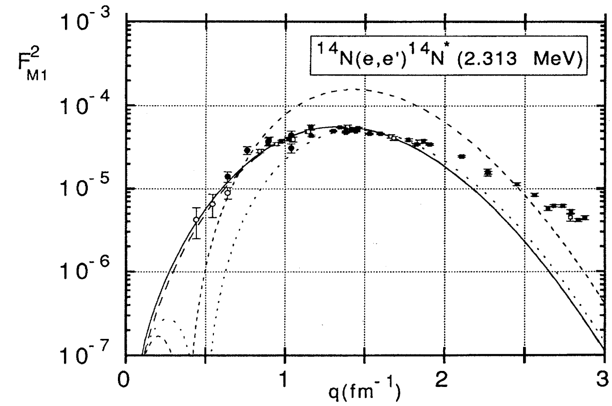

FIG. 5. ^{14}N 2.313 MeV $M1$ (e,e') form factor: RPI-N2 (solid curve), $H1$ (long-dashed curve), Cohen-Kurath (short-dashed curve), and Cohen-Kurath with $\Phi_{21;11}/2$ (dotted curve). The data are from Ref. [10] (open circles), Ref. [3] (solid circles), Ref. [5] (open squares), and Ref. [9] (solid squares).

Kurath $\Phi_{21;11}$ TDME, one still finds a diffraction minimum near $q = 0.5$ fm^{-1} in the inelastic form factor, which is not seen experimentally.

We perform fits similar to RPI-N2 except with the $\Phi_{01;11}$ or $\Phi_{10;11}$ considered as free parameters. This yields R_{01} and R_{10} on the order of unity, which indicates that the fits cannot determine any renormalization for these TDME's. Also, repeating this procedure for the "conjugate" nucleus ^{6}Li yields no renormalization of $\Phi_{21;11}$. Note that RPI-N2 yields a better value for T_γ^{M1}. Also, Q is at 50% of the experimental value, consistent with the 50% renormalization of the $L=2,S=1$ strength. We show with Wittman that RPI-N2 is consistent with the ^{14}N$_{\text{g.s.}}$ (γ,π^+) ^{14}C$_{\text{g.s.}}$ reaction at low energy [17].

VI. CONCLUSION

We have examined the $1p$-shell structure of the $A = 6$, 12, and 14 systems and have found electroweak observables that yield effective one-body amplitudes characteristic of this structure. We have used the latest database, in conjuction with the powerful CERN fitter routine, MINUIT, to search for the optimum fit for the one-body amplitudes. Our procedure works best when significant two-body effects are not present, or are effectively taken into account, as with the renormalization of the transition density reduced matrix element $\Phi_{21;11}$, in the $A = 14$ case. We have also explored the limits of our procedure as a function of momentum transfer, finding the boundary between one-body and two-body physics in the electroweak transitions in light nuclei.

Our optimized fits, denoted RPI-L, RPI-C2, and RPI-N2, can now be used with other processes dominated by one-body physics. Such a test of these effective one-body amplitudes is given in our companion study of the pion photoproduction reaction at low energy, with Wittman [17], where our derived nuclear amplitudes fare very well when compared with experiments.

ACKNOWLEDGMENTS

Our research at Rensselaer has been supported by the U.S. Department of Energy. We are grateful to M. Benmerrouche, J. Dubach, T. W. Donnelly, B. Goulard, D. Kurath, T.-S. H. Lee, and R. S. Wittman for helpful discussions and communications. We thank our Rensselaer experimental colleagues for their interest.

[1] T. W. Donnelly and J. D. Walecka, Phys. Lett. **44B**, 330 (1973).
[2] B. Jancovici and I. Talmi, Phys. Rev. **95**, 289 (1954).
[3] N. Ensslin, W. Bertozzi, S. Kowalski, C. P. Sargent, W. Turchinetz, C. F. Williamson, S. P. Fivozinsky, J. W. Lightbody, Jr., and S. Penner, Phys. Rev. C **19**, 569 (1979).
[4] B. Goulard, B. Lorazo, H. Primakoff, and J. Vergados, Phys. Rev. C **16**, 1999 (1977).
[5] R. L. Huffman, J. Dubach, R. S. Hicks, and M. A. Plum, Phys. Rev. C **35**, 1 (1987).
[6] J. C. Bergstrom, I. P. Sauer, and R. S. Hicks, Nucl. Phys. **A251**, 401 (1975).
[7] J. C. Bergstrom, S. B. Kowalski, and R. Neuhausen, Phys. Rev. C **25**, 1156 (1982).
[8] J. C. Bergstrom, U. Deutschmann, and R. Neuhausen, Nucl. Phys. **A327**, 439 (1979).
[9] R. L. Huffman, R. S. Hicks, J. Dubach, B. Parker, M. A. Plum, G. Lahm, R. Neuhausen, and J. C. Bergstrom, Phys. Lett. **139B**, 249 (1984).
[10] N. Ensslin *et al.*, Phys. Rev. C **9**, 1705 (1974).
[11] B. T. Chertok, C. Sheffield, J. W. Lightbody, Jr., S. Penner, and D. Blum, Phys. Rev. C **8**, 23 (1973).
[12] U. Deutschmann, G. Lahm, and R. Neuhausen, Nucl. Phys. **A411**, 337 (1983).

[13] L. Lapikás, in Proceedings of the Conference on Modern Trends in Elastic Electron Scattering, Amsterdam, The Netherlands, 1978 (unpublished).
[14] See, for example, J. F. Mathiot, Phys. Rep. **173C**, 63 (1989).
[15] W. C. Haxton, Phys. Lett. **76B**, 165 (1978).
[16] J. S. O'Connell, T. W. Donnelly, and J. D. Walecka, Phys. Rev. C **6**, 719 (1972).
[17] B. C. Doyle, N. C. Mukhopadhyay, and R. S. Witten, the following paper, Phys. Rev. C **52**, 1957 (1995).
[18] A. Bohr and B. Mottelson, *Nuclear Structure* (W. A. Benjamin Inc., New York, 1969), Vol. I.
[19] T.-S. H. Lee and D. Kurath, Phys. Rev. C **21**, 293 (1980); we use the (8-16)POT amplitude for mass 14.
[20] B. Doyle, B. Goulard, and N. C. Mukhopadhyay, Phys. Rev. C **42**, 1361 (1990).
[21] M. K. Singham, Nucl. Phys. **A460**, 597 (1986).
[22] K. Amos, D. Koetsier, and D. Kurath, Phys. Rev. C **40**, 374 (1989).
[23] N. C. Mukhopadhyay, Phys. Rev. C **6**, 1720 (1973).
[24] N. C. Mukhopadhyay and J. Martorell, Nucl. Phys. **A296**, 461 (1978).
[25] Review of Particle Properties, Phys. Rev. D **45**, S1 (1992).
[26] D. Vautherin and D. M. Brink, Phys. Rev. C **5**, 626 (1972).
[27] X. Campi and D. Sprung, Nucl. Phys. **A194**, 401 (1972).
[28] M. A. Preston, *Physics of the Nucleus* (Addison-Wesley, Reading, MA, 1962).
[29] Review of Particle Properties, Phys. Lett. **170B**, 1 (1986); the 1992 Particle Data Group values [25] of G and $g_A(0)$ result in less than a 1% difference in Eq. (20).
[30] F. James and M. Roos, computer code MINUIT, CERN Program Library entry D506, Geneva, Switzerland, 1989.
[31] S. Cohen and D. Kurath, Nucl. Phys. **73**, 1 (1965).
[32] F. Ajzenberg-Selove, Nucl. Phys. **A336**, 1 (1980).
[33] H. De Vries, C. W. De Jager, and C. De Vries, At. Data Nucl. Data Tables **36**, 495 (1987).
[34] J. Dubach and W. Haxton, Phys. Rev. Lett. **41**, 1453 (1978).
[35] R. S. Hicks, R. L. Huffman, R. A. Lindgren, G. A. Peterson, M. A. Plum, and J. Button-Shafer, Phys. Rev. C **36**, 485 (1987).
[36] F. Ajzenberg-Selove, Nucl. Phys. **A431**, 1 (1984).
[37] F. Ajzenberg-Selove, Nucl. Phys. **A490**, 1 (1988).
[38] F. Ajzenberg-Selove, Nucl. Phys. **413**, 1 (1984).
[39] F. Ajzenberg-Selove, Nucl. Phys. **A281**, 1 (1977).
[40] G. G. Ryzhikh, R. A. Eramzhhyan, V. I. Kukulin, and Yu. M. Tchuvil'sky, Nucl. Phys. **A563**, 247 (1993).
[41] F. Ajzenberg-Selove, Nucl. Phys. **A360**, 1 (1981).
[42] B. Doyle, in *International Workshop on Excited Baryons*, edited by G. Adams, N. C. Mukhopadhyay, and P. Stoler (World Scientific, Singapore, 1989), p. 373.
[43] B. H. Cottman *et al.*, Phys. Rev. Lett. **55**, 684 (1985).
[44] R. S. Wittman and N. C. Mukhopadhyay, Phys. Rev. Lett. **57**, 1113 (1986).
[45] K. Röhrich, G. Köbschall, C. Reifferscheid, C. Schmitt, V. H. Walther, and K. Weinand, Nucl. Phys. **A475**, 761 (1987).
[46] C. Bennhold and L. Tiator, Phys. Rev. C **42**, 464 (1990).